Multimode Hydrodynamic Instability Growth of Preimposed Isolated Defects in Ablatively Driven Foils

C. Zulick[©],[*] Y. Aglitskiy, M. Karasik, A. J. Schmitt, A. L. Velikovich[©], and S. P. Obenschain

Naval Research Laboratory, Washington, D.C. 20375, USA

The Nike KrF laser facility was used to study the evolution of isolated defects with characteristic sizes of < 1 to 10s of μm in laser-accelerated plastic foils. The experimental platform permitted, for the first time, the systematic study of localized perturbation growth, which is inherently multimode, through ablative Richtmyer-Meshkov and Rayleigh-Taylor stages and into the strongly nonlinear regime. Initial target defects were relatively large amplitude, but spatially localized, and emulated tent, fill-tube, and other nonuniformities that are present in inertial confinement fusion capsules. Face-on x-ray radiography indicated initial growth of the perturbation in both depth and width, followed by its apparent closure due to oblique spike growth. Hollow jetlike profiles of laterally expanding, rising, Rayleigh-Taylor bubbles were observed on the rear surface of the target from each isolated defect. Radiation hydrodynamic simulations provided insight into the mechanism of the closure and other features of the bubble and spike evolution specific to isolated defects.

Ablatively accelerated inertial confinement fusion targets are subject to hydrodynamic instabilities, which lead to the growth of nonuniformities. This growth can result in asymmetric target compression and mixing of the ablator material into the fuel, degrading the target uniformity at stagnation [1–3]. Recent experiments on the NIF and OMEGA have raised questions about the effect of isolated large-amplitude perturbations such as fill tubes [4,5], direct-drive [6] and indirect-drive [7,8] target mount structures, pits, and other localized target defects [9–11] on target performance. Several engineering approaches have been investigated [12–15] to reduce perturbations by minimizing the size of defects. Defect-induced mix experiments (DIME) on OMEGA [16,17] and NIF [18] measured and modeled the influence of localized defects (equatorial grooves) on P_2 asymmetry at stagnation and neutron yields which showed that modeling of the fine-scale interaction of the groove feature is a very challenging task [16–18]. There is extensive literature on strong-shock-driven flows affected by localized preshock nonuniformities and structures, including distortion of shock fronts and formation of jets [19,20]. However, these studies do not directly address the growth of the bubbles and spikes, the lateral mass redistribution, or similar instability manifestations that start from small seeds and cause the target distortion and mix.

The seeding and growth of perturbations in laser-driven targets has been studied for many years; see the reviews [2,21–23] and references therein. Distortion of the targets, seeded by their imperfections or the irradiation nonuniformity, typically starts from small initial amplitudes and proceeds through an oscillatory early-time evolution before the target starts accelerating, the Richtmyer-Meshkov instability (RMI), and is then amplified via the Rayleigh-Taylor instability (RTI). The smallness of the initial amplitudes makes it possible to Fourier-decompose the perturbation and study each mode separately, as in [24]. When the phases of the Fourier modes are random, which is the case for surface roughness or laser imprint, the mode coupling begins at the nonlinear stage leading to harmonic generation, bubble competition, and bubble merger.

Much less is known about the seeding and growth of perturbations from isolated target defects when the above physical picture is inapplicable. Starting from the small-amplitude phase, the growth is inherently multimode, involving a large number of phase-locked Fourier modes. Moreover, a bubble developed from an isolated indentation does not merge or compete with its neighbors because there are none. Its nonlinear evolution is, therefore, specific to the isolated case. Publications on the subject are relatively few, with an analytical work on the nonlinear classical RTI growth of an isolated divot on a thin fluid layer [25], and simulations [10] describing the ablative RMI [26,27] and RTI evolution of a single bump. In experiments, indirectly driven planar targets with periodic arrays of surface bumps were observed through the ablative RMI stage [9]. More work is needed to elucidate both the linear and nonlinear physics of isolated perturbation evolution.
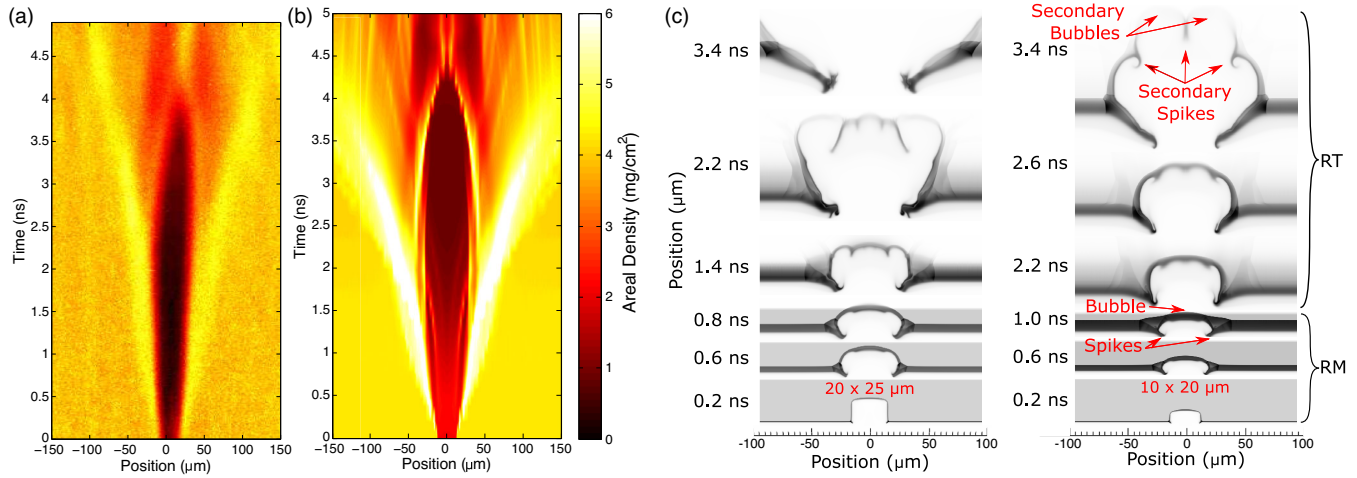
FIG. 1. Streaked areal density from (a) experiment and (b) simulation for a 20 μm deep by 25 μm wide defect. Plasma density maps of two defects, size as indicated, from FASTRAD3D (c) at specified times showing formation of the rising bubble and the oblique spikes as well as the lateral bubble expansion responsible for the expanding light area in the streaked image.

This Letter reports the results of the first direct systematic experimental and numerical study of the hydrodynamic growth of isolated defects in ablatively driven targets, and provides the first experimental observation of effects predicted in early analytical work and simulations [28,29]. The work was performed with planar plastic targets ablatively accelerated by the Nike krypton-fluoride (KrF) laser [30]. The 248 nm laser radiation was focused to a 750 μm focal spot, with a 400 μm flat top profile, and less than 2% rms energy variation in each of the 40 overlapping beams. The uniformity of the Nike laser drive was made possible by induced spatial incoherence [31,32] and ensured that the observed perturbation growth was caused mostly by the target defects. A 4 ns square pulse at a peak intensity of 5–8×10^{13} W/cm^2 was used to drive the targets.

The targets were solution-cast polystyrene foils machined at NRL using a 10 kHz repetition rate 500 femtosecond duration laser to produce isolated defects, as described in detail in the Supplemental Material [33], which includes Refs. [34,35]. This technique allowed precise ablation of the CH material without significant heating of the periphery of the laser machined grooves, minimizing density discontinuities and gradients. The defects were straight grooves machined with lengths of 500 μm, depths of 0.1 to 30 μm, and widths of 1 to 25 μm. Targets were produced with either a single groove or a set of three parallel grooves spaced 150 μm apart. Our parameter range overlaps with and extends, towards smaller scales, that of previous studies [9,16–18]

The target was oriented normal to the laser axis with the defects on the laser side. The two primary diagnostics were monochromatic x-ray imagers using spherically bent crystals [36] backlit at 1.865 keV with spatial resolutions of 10 μm. Face-on areal density measurement were made with a backlighter target located 25 degrees off of target normal

in the plane of the groove. The grooves were imaged with a magnification of 14.5 to the slit of an 80 ps resolution streak camera such that a perpendicular slice was measured through the groove(s). A 5 ns backlighter was used to produce streaked face-on images over the entire duration of the main pulse. The side-on diagnostic utilized BAS-TR image plate to record two-dimensional (2D) images with a magnification of 12.3 and was aligned along the target surface plane and 500 μm groove length. A backlighter pulse as short as 500 ps was used to produce a "snap-shot" of the target at a specific time delay.

The use of monoenergetic backlighters allowed calculation of the areal density using the mass attenuation coefficient and the known thickness of the unperturbed target. Deconvolution using a Gaussian line spread function was used to deblur the face-on streaked image along the spatial axis of the streak camera. This algorithm was validated against a streaked image of an undriven target with a 14 μm deep by 10 μm wide groove and reduced the error of the areal density measurement to less than 10%.

Figure 1(a) is a processed streaked face-on image showing the time evolution of the areal density which is spatially resolved in the direction perpendicular to a 20 μm deep by 25 μm wide groove. It appears to indicate two distinct stages. At first, the darker central area, indicating reduced areal density near the centerline of the initial indentation, increases in width and depth up to $\approx$2 ns, before and after the ablative RTI growth begins at the simulated shock breakout time of $\approx$1.25 ns. Then the dark void is seen to shrink, almost closing at $\approx$3 ns, while the RTI growth continues until the laser pulse shuts off at 4 ns. The initial "scar" on the target appears to be self-healing, making the accelerated foil appear more uniform instead of the being cut through. At the same time, the lighter peripheral area indicating increased areal density keeps expanding throughout the pulse.
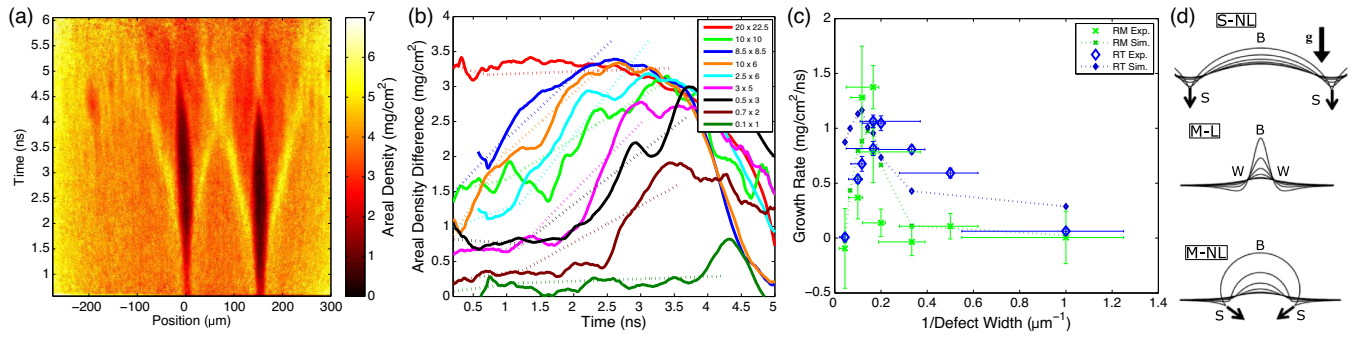
FIG. 2. Streaked areal density (a) of a target with grooves of dimensions 0.1×1, 2.5×6, and 8.5×8.5 deep (μm) × wide (μm). Linear plot (b) of the target areal density perturbation amplitude along the isolated defect centerline. The experimental data (solid line) is compared to RM and RT growth fitting (dotted). (c) Linear RM and RT fitted growth rates as a function of inverse defect width along with simulated fits (dashed). (d) Schematic of the RT growth in a thin layer: Ott's model [28] for single-mode nonlinear (S-NL); multimode linear (M-L); and multimode nonlinear (M-NL) for an isolated 2D perturbation.

To explain this rather unexpected behavior, we turn to high-resolution 2D numerical simulations done with the NRL compressible radiation-hydrodynamics code, FASTRAD3D [37]. The code was validated against our extensive experimental data on both ablative and classical RTI and Richtmyer-Meshkov instabilities, see [21,38] and references therein.

Figure 1(b) shows a synthetic areal-density streak image simulated in 2D for the experimental conditions of Fig. 1(a). This simulation ignores target surface roughness and laser drive nonuniformity and uses the isolated groove as the only perturbation source. Qualitative features of Fig. 1(a) discussed above were all reproduced, with the timing and spatial dimensions close to the observations. The sequence of side-on density maps generated in the simulation, Fig. 1(c), help understand what is going on.

During the shock-rarefaction transit time, that is, before ≈ 1.25 ns, surface perturbations are subject to the ablative RM instability [21,26,27]. The RM bubble developed from the initial rectangular groove rises through the shocked material while the shock front propagates to the rear surface of the target. The onset of acceleration triggers ablative RT growth. The RT bubble rises into the vacuum, ahead of the rest of the target. The areal-density measurements detect both phases, seen in Fig. 2(b), but the side-on density maps of Fig. 1(c) do not reveal any qualitative distinction between the RM and RT phases of the perturbation evolution. Throughout the laser pulse, the thin-walled bubble is seen to expand both laterally and vertically. Its growth is accompanied by mass ejection into the spikes, as expected. However, they do not fall vertically, as in the single-mode regime. Instead, the spikes on both sides of the bubble grow obliquely, gradually increasing the angle between their plane and the vertical direction of acceleration. Such behavior of the spikes was first detected in the analytical study of the nonlinear RT instability of an isolated divot, see Fig. 3 of Ref. [25]. The roll-ups at the tips of the spikes is produced by the secondary Kelvin-Helmholtz (KH) instability at the mushrooming stage

of the nonlinear RM and RT instability development [22,23]. The movement of the spike mass into the face-on field of view, towards the centerline, produces the apparent closure of the dark void in Figs. 1(a) and 1(b). The lateral expansion of the bubble pushes some target mass that has not yet entered the spike away from the centerline, producing the increased areal density seen face-on in Figs. 1(a) and 1(b) as the expanding lighter area.

The tip of the simulated rising bubbles in Fig. 1(c) exhibits a secondary RT instability, developing smaller bubbles. The instability is a feature specific to the acceleration of a thin layer. The tip of a bubble rising through a dense fluid is stabilized by the fluid flow past its surface, as first shown for the classical RT instability [39] and then confirmed in many simulation and experiments for both classical and ablative cases [22,23,40]. There is no such stabilization in the thin-layer case, hence the instability. The secondary bubbles evolve the same way as the primary bubble, expanding in both directions and ejecting mass into oblique spikes with roll-ups.

Figure 2(a) shows a streak image for a target with three defects of initial sizes of 0.1×1, 2.5×6, and 8.5×8.5 deep (μm) × wide (μm). The centerline of each defect was used to characterize the temporal evolution of the areal mass perturbation amplitude associated with this defect. The lineouts for nine such defects are shown in Fig. 2(b) as solid curves. In Fig. 2(b), we do not, uniformly, see a substantial increase in the growth rate as the flow evolves from the RM to the RT phase.

The nonlinearity parameter for a single-mode perturbation is defined as $k\nu$, where k and ν are the wave number and the mode amplitude, respectively. Modifying this parameter for isolated defects as $2\pi d/w$, where d and w are the depth and width of the groove, respectively, we find that for the conditions of our experiment the initial value of this parameter varies in the range of ≈ 1 to 10, indicating that the RM and RT growth is nonlinear from the beginning. We chose to fit the evolution of the areal-mass
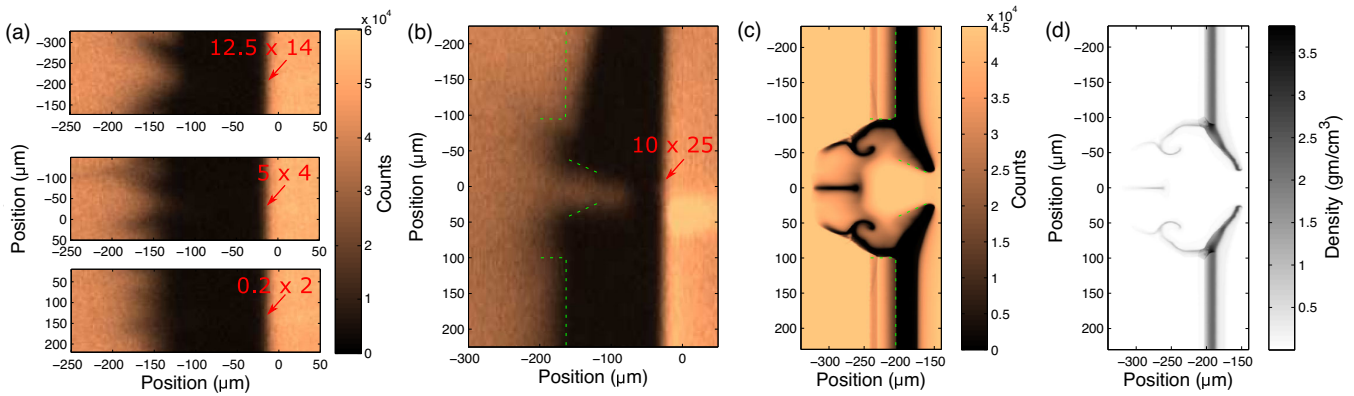
FIG. 3. Side-on image at 2 ns of three machined defects (a) showing rear surface jets. Initial isolated defect feature size and location are indicated. A narrow (500 μm wide) target shows (b) the machined defect produced a large indentation in the accelerated target at 4 ns. FASTRAD3D simulations show the same indentation and qualitative appearance in the transmitted backlighter signal (c) corresponding to the simulated plasma density map (d). The laser enters from the right side of the images and self-emission is evident in (b).

perturbation amplitude during both the RM and RT phases with linear functions, $\delta m = ut + \delta m_0$, where u and m_0 are dimensional fitting coefficients. The fits were performed from $t_0 = 0$ to the scaled shock breakout time, $t_1 = [1 - (d/40~\mu m)]1.25$ ns, and then to t_2 at the peak amplitude. The fitting curves are shown in Fig. 2(b) as dotted lines, and the experimental rate coefficients u (mg/cm^2/ns) are presented in Fig. 2(c) along with the simulation growth rates. The growth rates peak around $(6~\mu m)^{-1}$ and decrease for both wider and narrower grooves due to saturation and reduced growth rates, respectively.

The observed perturbation growth in all cases is the deformation of a thin layer due to a nonuniform mass flow. It represents the evolution of two counter-rotating vortex sheets produced on both sides of the central bubble. This effect is schematically illustrated in Fig. 2(d) with the aid of the Ott's solution for nonlinear RT growth in a thin fluid layer [28], on which the analysis of Ref. [25] is based. Here, this solution is appropriately modified for an isolated defect. The top sketch labeled S-NL illustrates the nonlinear development of a single-mode perturbation and reproduces Ott's Fig. 1. It shows a time sequence of trochoidal shapes of the layer, where the bubble and spike are labeled B and S, respectively. As argued in [28,41,42], the bubble part of the solution remains a fair approximation while the collision of the neighboring bubbles makes most of the colliding mass flow into thin spikes similar to the dense slugs described for collision of incompressible thin layers in [43]. Due to the symmetry of the single-mode case, the spikes fall vertically down.

The sequence of layer shapes labeled M-L in Fig. 2(d) illustrates the multimode linear, or small amplitude, case for a Lorentzian shape of the initial perturbation. Due to the faster growth rates of the short-wavelength Fourier modes, the upward growth of the bubble is accompanied by the downward growth of the "wings" labeled W. The mass flows into the wings in opposite directions from the bubble

and the horizontal layer on the other side. The nonlinear case marked M-NL allows for a lateral expansion of the bubble, which leads to its collision with the wing. The oppositely directed mass flows of different magnitude form two counter-rotating vortex sheets and drive mass into the spikes that are oblique rather than vertical. Asymmetry of the mass flows makes the spike tips roll up. The same happens when the walls of the secondary bubbles collide, as seen in Fig. 1(c). For the rotationally symmetric divot defect [25] there is a single toroidal vortex ejecting the spike mass obliquely.

Figure 3 displays isolated bubbles observed side on. Figure 3(a) presents an image of a target with three groove defects backlit from 2 to 2.75 ns showing dual, bifurcated, hollow-jet-like structures emerge from each defect. A smooth rear surface was observed at 4 ns in a control shot of a target with no machined defects. The structures seen in Fig. 3(a) are not true jets, like those discussed in [20, 43–47], i.e., collimated mass flows, which expand in the lateral direction slower than they propagate. In contrast, the hollow structures in Fig. 3(a) are side-on images of the RT bubbles, which inflate while rising or bursting. A parameter scan of targets with defects ranging from 0.2 to 20 μm deep and 1 to 14 μm wide showed that the structures formed after shock breakout and the largest structures grew in size from 100 μm at 2 ns to 200 μm at 3.5 ns, demonstrating significant lateral growth. Their observed lateral expansion is a new feature of the bubbles growing from isolated defects, as explained above.

An image of a narrow, 500 μm wide, target with a 10 μm × 25 μm groove is shown in Fig. 3(b), which allowed for the observation of the interior of the defect by removing the unaccelerated width of the wider targets. Synthetic side-on images generated from 2D FASTRAD3D simulation results are shown in Figs. 3(c) and 3(d). The bubble width was uniform along the length of the groove, which allowed direct imaging of its sides due to the

increased areal density seen by the side-on diagnostic. However, the tip of the bubble, i.e., the portion of the bubble accelerated far in front of the target, was not imaged experimentally. This was likely due to mass loss from the bubble and fluctuations in the location of the tip, seeded by instability growth and machined groove depth variations, reducing the areal density below observable limits. Figures 3(b) and 3(c) have been overlaid with equivalent dashed green lines, positioned relative to the unperturbed target surface, showing the location of the bubble wall and the oblique spikes.

To summarize, the inherently multimode hydrodynamic growth of isolated defects in laser-driven targets has been measured for the first time using face-on streaked areal density and side-on imaging. Lateral expansion of the rising RT bubble, a newly discovered feature of bubbles growing from isolated defects, was observed in side-on images of the rear target surface. Simulations demonstrated the apparent closure of the growing bubble void in the face-on observations resulted from the mass ejected into oblique spikes moving into the field of view. The oblique spikes were formed from the collision between the laterally expanding primary bubble and the trailing mass on its sides. Nonuniform mass flow in the bubble walls created counter-rotating vortex sheets, ejecting the spikes in the oblique direction and producing roll-ups at their tips.

Our findings lead to the general observation that areal density measurements by themselves are an insufficient diagnostic for characterizing the impact of isolated defects in inertial confinement fusion experiments, and in fact, can under represent the impact of the defects on the target integrity. Our present results are only the beginning of the systematic experimental studies of perturbation growth triggered by isolated defects that could be carried out on Nike and other laser facilities, with both direct and indirect drive. It is important to investigate perturbation growth from rotationally symmetric "dot" defects, similar to that modeled in [10] but with an initial indentation instead of a bump. With localized defects placed at the rear target surface, one can study the areal mass evolution in a perturbed expansion wave or RM jet formation, as done for the single mode cases in Refs. [27] and [48], respectively.

---

[*]calvin.zulick@nrl.navy.mil

[1] S. E. Bodner, D. G. Colombant, J. H. Gardner, R. H. Lehmberg, S. P. Obenschain, L. Phillips, A. J. Schmitt, J. D. Sethian, R. L. McCrory, W. Seka, C. P. Verdon, J. P. Knauer, B. B. Afeyan, and H. T. Powell, Direct-drive laser fusion: Status and prospects, Phys. Plasmas **5**, 1901 (1998).

[2] R. S. Craxton *et al.*, Direct-drive inertial confinement fusion: A review, Phys. Plasmas **22**, 110501 (2015).

[3] A. B. Zylstra, S. MacLaren, S. A. Yi, J. Kline, D. Callahan, O. Hurricane, B. Bachmann, G. Kyrala, L. Masse, P. Patel, J. E. Ralph, J. Salmonson, P. Volegov, and C. Wilde, Implosion performance of subscale beryllium capsules on the nif, Phys. Plasmas **26**, 052707 (2019).

[4] A. G. MacPhee, D. T. Casey, D. S. Clark, S. Felker, J. E. Field, S. W. Haan, B. A. Hammel, J. Kroll, O. L. Landen, D. A. Martinez, P. Michel, J. Milovich, A. Moore, A. Nikroo, N. Rice, H. F. Robey, V. A. Smalyuk, M. Stadermann, and C. R. Weber, X-ray shadow imprint of hydrodynamic instabilities on the surface of inertial confinement fusion capsules by the fuel fill tube, Phys. Rev. E **95**, 031204(R) (2017).

[5] A. MacPhee, V. Smalyuk, O. Landen, C. Weber, H. Robey, E. Alfonso, K. Baker, L. Berzak Hopkins, J. Biener, T. Bunn *et al.*, Hydrodynamic instabilities seeded by the x-ray shadow of icf capsule fill-tubes, Phys. Plasmas **25**, 082702 (2018).

[6] I. Igumenshchev, F. Marshall, J. Marozas, V. Smalyuk, R. Epstein, V. Goncharov, T. Collins, T. Sangster, and S. Skupsky, The effects of target mounts in direct-drive implosions on omega, Phys. Plasmas **16**, 082701 (2009).

[7] S. R. Nagel, S. W. Haan, J. R. Rygg, M. Barrios, L. R. Benedetti, D. K. Bradley, J. E. Field, B. A. Hammel, N. Izumi, O. S. Jones, S. F. Khan, T. Ma, A. E. Pak, R. Tommasini, and R. P. J. Town, Effect of the mounting membrane on shape in inertial confinement fusion implosions, Phys. Plasmas **22**, 022704 (2015).

[8] V. A. Smalyuk, C. R. Weber, H. F. Robey, D. T. Casey, K. Chen, D. S. Clark, M. Farrell, S. Felker, J. E. Field, S. W. Haan, B. A. Hammel, A. V. Hamza, D. Hoover, J. J. Kroll, O. L. Landen, A. G. MacPhee, D. Martinez, A. Nikroo, and N. Rice, Hydrodynamic instability growth of three-dimensional modulations in radiation-driven implosions with "low-foot" and "high-foot" drives at the national ignition facility, Phys. Plasmas **24**, 042706 (2017).

[9] E. N. Loomis, D. Braun, S. H. Batha, C. Sorce, and O. L. Landen, Areal density evolution of isolated surface perturbations at the onset of x-ray ablation richtmyer-meshkov growth, Phys. Plasmas **18**, 092702 (2011).

[10] I. V. Igumenshchev, V. N. Goncharov, W. T. Shmayda, D. R. Harding, T. C. Sangster, and D. D. Meyerhofer, Effects of local defect growth in direct-drive cryogenic implosions on omega, Phys. Plasmas **20**, 082703 (2013).

[11] W. T. Shmayda, D. R. Harding, V. A. Versteeg, C. Kingsley, M. Hallgren, and S. J. Loucks, Micron-scaled defects on cryogenic targets: An assessment of condensate sources, Fusion Sci. Technol. **63**, 87 (2013).

[12] C. R. Weber *et al.*, Improving ICF implosion performance with alternative capsule supports, Phys. Plasmas **24**, 056302 (2017).

[13] D. A. Martinez *et al.*, Hydro-instability growth of perturbation seeds from alternate capsule-support strategies in indirect-drive implosions on national ignition facility, Phys. Plasmas **24**, 102707 (2017).

[14] A. MacPhee, V. Smalyuk, O. Landen, C. Weber, H. Robey, E. Alfonso, J. Biener, T. Bunn, J. Crippen, M. Farrell *et al.*,

Mitigation of x-ray shadow seeding of hydrodynamic instabilities on inertial confinement fusion capsules using a reduced diameter fuel fill-tube, Phys. Plasmas **25**, 054505 (2018).

[15] V. Smalyuk, H. Robey, C. Alday, P. Amendt, C. Aracne-Ruddle, J. Bigelow, T. Bunn, D. Casey, K.-C. Chen, D. Clark *et al.*, Review of hydro-instability experiments with alternate capsule supports in indirect-drive implosions on the national ignition facility, Phys. Plasmas **25**, 072705 (2018).

[16] G. R. Magelssen, J. A. Cobble, I. L. Tregillis, M. J. Schmitt, S. H. Batha, P. A. Bradley, and K. A. D. Obrey, Single-shell direct-drive capsule designs to study effects of perturbations on burn, J. Phys. Conf. Ser. **244**, 022006 (2010).

[17] P. A. Bradley, J. A. Cobble, I. L. Tregillis, M. J. Schmitt, K. D. Obrey, V. Glebov, S. H. Batha, G. R. Magelssen, J. R. Fincke, S. C. Hsu, N. S. Krasheninnikova, T. J. Murphy, and F. J. Wysocki, Role of shocks and mix caused by capsule defects, Phys. Plasmas **19**, 092703 (2012).

[18] M. J. Schmitt *et al.*, Development of a polar direct-drive platform for studying inertial confinement fusion implosion mix on the national ignition facility, Phys. Plasmas **20**, 056310 (2013).

[19] S. R. Goldman, S. E. Caldwell, M. D. Wilke, D. C. Wilson, C. W. Barnes, W. W. Hsing, N. D. Delamater, G. T. Schappert, J. W. Grove, E. L. Lindman, J. M. Wallace, R. P. Weaver, A. M. Dunne, M. J. Edwards, P. Graham, and B. R. Thomas, Shock structuring due to fabrication joints in targets, Phys. Plasmas **6**, 3327 (1999).

[20] P. A. Keiter, J. B. Elliott, B. E. Blue, J. H. Cooley, J. Edwards, G. A. Kyrala, H. F. Robey, B. Spears, and D. C. Wilson, Measurement and simulation of jet mass caused by a high-aspect ratio hole perturbation, Phys. Plasmas **17**, 062704 (2010).

[21] Y. Aglitskiy, A. Velikovich, M. Karasik, N. Metzler, S. Zalesak, A. Schmitt, L. Phillips, J. Gardner, V. Serlin, J. Weaver, and S. Obenschain, Basic hydrodynamics of Richtmyer–Meshkov-type growth and oscillations in the inertial confinement fusion-relevant conditions, Phil. Trans. R. Soc. A **368**, 1739 (2010).

[22] Y. Zhou, Rayleigh–Taylor and Richtmyer–Meshkov instability induced flow, turbulence, and mixing. I, Phys. Rep. **720–722**, 1 (2017).

[23] Y. Zhou, Rayleigh–Taylor and Richtmyer–Meshkov instability induced flow, turbulence, and mixing. II, Phys. Rep. **723–725**, 1 (2017).

[24] C. E. Niederhaus and J. W. Jacobs, Experimental study of the Richtmyer-Meshkov instability of incompressible fluids, J. Fluid Mech. **485**, 243 (2003).

[25] M. M. Basko, Rayleigh–Taylor eigenmodes of a thin layer in the nonlinear regime, Phys. Plasmas **1**, 1270 (1994).

[26] V. N. Goncharov, Theory of the Ablative Richtmyer-Meshkov Instability, Phys. Rev. Lett. **82**, 2091 (1999).

[27] Y. Aglitskiy, A. L. Velikovich, M. Karasik, V. Serlin, C. J. Pawley, A. J. Schmitt, S. P. Obenschain, A. N. Mostovych, J. H. Gardner, and N. Metzler, Direct Observation of Mass Oscillations Due to Ablative Richtmyer-Meshkov Instability in Plastic Targets, Phys. Rev. Lett. **87**, 265001 (2001).

[28] E. Ott, Nonlinear Evolution of the Rayleigh-Taylor Instability of a Thin Layer, Phys. Rev. Lett. **29**, 1429 (1972).

[29] J. P. Dahlburg, J. H. Gardner, G. D. Doolen, and S. W. Haan, The effect of shape in the threedimensional ablative ray-leightaylor instability. I: Singlemode perturbations, Phys. Fluids B **5**, 571 (1993).

[30] S. Obenschain, S. Bodner, D. Colombant, K. Gerber, R. Lehmberg, E. McLean, A. Mostovych, M. Pronko, C. Pawley, A. Schmitt *et al.*, The Nike KrF laser facility: Performance and initial target experiments, Phys. Plasmas **3**, 2098 (1996).

[31] R. Lehmberg and S. Obenschain, Use of induced spatial incoherence for uniform illumination of laser fusion targets, Opt. Commun. **46**, 27 (1983).

[32] S. P. Obenschain, J. Grun, M. J. Herbst, K. J. Kearney, C. K. Manka, E. A. McLean, A. N. Mostovych, J. A. Stamper, R. R. Whitlock, S. E. Bodner, J. H. Gardner, and R. H. Lehmberg, Laser-Target Interaction with Induced Spatial Incoherence, Phys. Rev. Lett. **56**, 2807 (1986).

[33] See the Supplemental Material at http://link.aps.org/supplemental/10.1103/PhysRevLett.125.055001 for details of machining isolated defects in polystyrene foils, which includes Refs. [34,35].

[34] J. Grun, C. K. Manka, S. Nikitin, D. Zabetakis, G. Comanescu, D. Gillis, and J. Bowles, Identification of bacteria from two-dimensional resonant-raman spectra, Anal. Chem. **79**, 5489 (2007).

[35] J. C. Wyant, White light interferometry, in *Holography: A Tribute to Yuri Denisyuk and Emmett Leith* (International Society for Optics and Photonics, Bellingham, 2002), Vol. 4737, pp. 98–107.

[36] Y. Aglitskiy, T. Lehecka, S. Obenschain, S. Bodner, C. Pawley, K. Gerber, J. Sethian, C. M. Brown, J. Seely, U. Feldman *et al.*, High-resolution monochromatic x-ray imaging system based on spherically bent crystals, Appl. Opt. **37**, 5253 (1998).

[37] J. W. Bates, A. J. Schmitt, M. Karasik, and S. T. Zalesak, Numerical simulations of the ablative rayleigh-taylor instability in planar inertial-confinement-fusion targets using the fastrad3d code, Phys. Plasmas **23**, 122701 (2016).

[38] Y. Aglitskiy, M. Karasik, A. L. Velikovich, V. Serlin, J. Weaver, T. J. Kessler, A. J. Schmitt, S. P. Obenschain, N. Metzler, and J. Oh, Observation of Strong Oscillations of Areal Mass in an Unsupported Shock Wave, Phys. Rev. Lett. **109**, 085001 (2012).

[39] P. Garabedian, On steady-state bubbles generated by taylor instability, Proc. R. Soc. A **241**, 423 (1957).

[40] H. Zhang, R. Betti, R. Yan, D. Zhao, D. Shvarts, and H. Aluie, Self-Similar Multimode Bubble-Front Evolution of the Ablative Rayleigh-Taylor Instability in Two and Three Dimensions, Phys. Rev. Lett. **121**, 185002 (2018).

[41] D. Colombant, W. Manheimer, and E. Ott, Three-Dimensional, Nonlinear Evolution of the Rayleigh-Taylor Instability of a Thin Layer, Phys. Rev. Lett. **53**, 446 (1984).

[42] W. Manheimer, D. Colombant, and E. Ott, Three-dimensional, nonlinear evolution of the rayleigh-taylor instability of a thin layer, Phys. Fluids **27**, 2164 (1984).

[43] G. Birkhoff, D. P. MacDougall, E. M. Pugh, and G. Taylor, Explosives with lined cavities, J. Appl. Phys. **19**, 563 (1948).

[44] M. B. Zellner, M. Grover, J. E. Hammerberg, R. S. Hixson, A. J. Iverson, G. S. Macrum, K. B. Morley, A. W. Obst, R. T.

Olson, J. R. Payton, P. A. Rigg, N. Routley, G. D. Stevens, W. D. Turley, L. Veeser, and W. T. Buttler, Effects of shock-breakout pressure on ejection of micron-scale material from shocked tin surfaces, J. Appl. Phys. **102**, 013522 (2007).

[45] G. Dimonte, G. Terrones, F. J. Cherne, T. C. Germann, V. Dupont, K. Kadau, W. T. Buttler, D. M. Oro, C. Morris, and D. L. Preston, Use of the Richtmyer-Meshkov Instability to Infer Yield Stress at High-Energy Densities, Phys. Rev. Lett. **107**, 264502 (2011).

[46] W. T. Buttler, D. M. Oro, D. L. Preston, K. O. Mikaelian, F. J. Cherne, R. S. Hixson, F. G. Mariam, C. Morris, J. B. Stone, G. Terrones *et al.*, Unstable richtmyer-meshkov growth of solid and liquid metals in vacuum, J. Fluid Mech. **703**, 60 (2012).

[47] S. P. Nikitin, J. Grun, Y. Aglitskiy, C. Manka, D. Zabetakis, A. L. Velikovich, and C. Miller, Production of cumulative jets by ablatively-driven implosion of hollow cones and wedges, Phys. Plasmas **15**, 050703 (2008).

[48] Y. Aglitskiy, M. Karasik, A. L. Velikovich, V. Serlin, J. L. Weaver, T. J. Kessler, S. P. Nikitin, A. J. Schmitt, S. P. Obenschain, N. Metzler, and J. Oh, Observed transition from Richtmyer-Meshkov jet formation through feedout oscillations to Rayleigh-Taylor instability in a laser target, Phys. Plasmas **19**, 102707 (2012).